2017 IEEE International Conference on Robotics and Automation (ICRA)
Singapore, May 29 - June 3, 2017

Magnetically Actuated Soft Capsule Endoscope for Fine-Needle Aspiration Biopsy

Donghoon Son[1], *Student Member, IEEE,* Mustafa Doga Dogan[2], *Student Member, IEEE,* and Metin Sitti[1], *Fellow, IEEE*

***Abstract*— This paper presents a magnetically actuated soft capsule endoscope for fine-needle aspiration biopsy (B-MASCE) in the upper gastrointestinal tract. A thin and hollow needle is attached to the capsule, which can penetrate deeply into tissues to obtain subsurface biopsy sample. The design utilizes a soft elastomer body as a compliant mechanism to guide the needle. An internal permanent magnet provides a means for both actuation and tracking. The capsule is designed to roll towards its target and then deploy the biopsy needle in a precise location selected as the target area. B-MASCE is controlled by multiple custom-designed electromagnets while its position and orientation are tracked by a magnetic sensor array. In *in vitro* trials, B-MASCE demonstrated rolling locomotion and biopsy of a swine tissue model positioned inside an anatomical human stomach model. It was confirmed after the experiment that a tissue sample was retained inside the needle.**

I. Introduction

Current medical technologies are converging to minimally invasive diagnosis and therapy [1]. In the diagnosis of gastrointestinal (GI) diseases, the efforts to reduce patient discomfort have resulted in the development of capsule endoscopes. Wireless capsule endoscopes, in the form of a pill, are well tolerated by patients, and they are currently used to collect diagnostic images and videos for the identification of suspicious lesions. They have even become the standard of care for some diagnostic procedures, such as the investigation of obscure GI bleeding [2]. While capsule endoscopy has already begun to revolutionize the diagnosis of GI disorders in the clinic, the possibilities afforded by capsule endoscopy are still being explored. One of the major limitations of commercially available devices is their inability to take biopsy samples after a suspicious lesion is identified. Acquiring a biopsy currently requires an additional endoscopic procedure, adding to the overall time and expense of making an accurate diagnosis. The ability to take biopsy samples is therefore a highly desirable addition to the feature set of capsule endoscopes [3].

Several capsule designs for taking biopsy samples have already been presented. The idea of taking biopsy samples in the GI tract with a small, swallowable device appeared as early as 1967 when an electromagnetic biopsy device was first presented by Driller and Neumann [4]. The capsule utilizes the peristalsis of the lower GI tract, air pressure through a tether, and an electromagnetically actuated razor inside the robot for cutting tissue. Kong *et al*. developed a rotational micro biopsy device [5], [6], which can cut sample tissues using a rotational razor inside the capsule, utilizing torsional springs (thermally or SMA triggered). Swain suggested a multiple capsule design in his patent [7], utilizing forceps or cutting razor-style biopsy tools through a narrow hole on the side of the capsule. Park *et al.* proposed a forceps-style biopsy tool actuated by a torsion spring, using a shape-memory alloy trigger [8]. Chen *et al.* suggested a forceps-style biopsy tool which is driven by a coil-based wireless power transfer system with double-balloon-enteroscopy-style locomotion [9]. Simi *et al.* integrated a magnetic torsion spring in a biopsy capsule that enables a blade to cut a tissue when the external magnetic field is removed [10].

Although most of the biopsy capsule designs have been created with lower GI tract applications in mind, it is possible that some of them may additionally work in the upper GI tract. One previous design has been specifically investigated for upper GI tract procedures. Yim *et al.* presented a magnetically actuated soft capsule endoscope (MASCE) with micro-grippers [11]. MASCE carries and deploys thermo-sensitive micro-grippers in the stomach and retrieves them with an adhesive patch after the micro-grippers grab the stomach tissues using its self-folding mechanism. However, experiments indicated that the yield of micro-gripper retrieval is low (3%), and in some cases a physician may prefer a targeted biopsy to the stochastic sampling performed by the micro-grippers.

Regardless of the location in the GI tract, one of the main limitations of all prior designs is that they can only take superficial biopsy samples. Those are useful to retract the tissues on the mucosal layer of the GI tract, however, it is difficult to reach deep masses inside the GI tract. Those mechanisms can miss submucosal tumors (SMTs), which can lower the diagnostic accuracy.

This paper presents a novel magnetically actuated soft capsule endoscope with fine-needle aspiration biopsy (FNAB) functionality called B-MASCE. FNAB is a type of biopsy technique to extract tissue samples using a fine needle. It was reported that fine-needle aspiration biopsy technique provides better accuracy than other biopsy techniques like forceps or brush, with the absence of complications in the GI tract [12], [13]. Because the needle can penetrate deep inside the mass of a lesion, this technique improves diagnostic

[1]Donghoon Son and Metin Sitti are with the Physical Intelligence Department, Max Planck Institute for Intelligent Systems, 70569 Stuttgart, Germany and the Department of Mechanical Engineering, Carnegie Mellon University, PA 15213 USA dhson@is.mpg.de and sitti@is.mpg.de

[2]Mustafa Doga Dogan is with the Department of Electrical and Electronics Engineering, Boğaziçi University, 34342 Istanbul, Turkey doga.dogan@boun.edu.tr

accuracy even in the case of SMTs.

The design of B-MASCE enables both the required motion for FNAB (axial jabbing motion of the needle) and rolling locomotion on the surface of a stomach. It is controlled by the magnetic force and torque on an internal magnet with external magnetic field control. Soft material-based legs connecting the two ends of the capsule work as a spring and a guide for the needle. The design is based on the clinical data suggesting the appropriate needle gauge and penetration depth for FNAB. *In vitro* experiments and a demonstration were performed with a swine tissue model, and it was verified that a biopsy sample was successfully captured.



Fig. 1. Prototype of B-MASCE. (a) B-MASCE with an anatomical stomach model and one Euro coin for size comparison. (b) B-MASCE faces ceiling by aligning it to the external magnetic field. (c) B-MASCE collapses with a strong gradient of the external magnetic field. The arrow indicates the exposed fine needle.

II. Application Scenario

A. Fine-Needle Aspiration Biopsy Technique

Fine-needle aspiration biopsy technique, also known as fine-needle aspiration cytology, describes the method of aspirating cells from suspicious tissue lesions through a thin and hollow needle. During the procedure, a hollow needle is inserted into a mass to extract samples of tissue. Once removed, they are sent to the laboratory for further examination. It is commonly used to investigate lumps located in the thyroid or the breast, and it has also been successfully applied in the GI tract [14].

There are two types of FNAB. During the so-called suction FNAB, a type of FNAB, the fine needle is passed into the tissue and a negative pressure is applied by means of a syringe attached to the needle. The second method is called fine-needle capillary (FNC) technique. The needle is passed into the tissue, and five to ten successive fast jabbing movements in and out of the tissue are performed [15]–[17]. The capillary force in the needle retains the detached cells inside the lumen. Clinical research has shown that there is no difference in terms of the diagnostic accuracy between the two techniques and it is recommended to use the FNC technique due to the technical ease [18].

FNAB has better diagnostic accuracy over forceps biopsy and brush cytology in GI tract applications [14], [19]–[21]. Clinical research by Zargar *et al.* has shown that FNAB outperforms the other two techniques in upper GI application (overall diagnostic accuracy: FNAB=94%, Brush=85%, Forceps=88%). Especially in case of submucosal tumors, infiltrative malignancies, and ulceronecrotic malignancies, FNAB is significantly better as the needle can penetrate deeply into the tumor mass while the other methods only capture superficial tissues of the stomach (e.g. diagnostic accuracy for SMT: FNAB=93%, Brush=7%, Forceps=14%) [12].

B. FNAB application on MASCE: B-MASCE

FNC technique is applied to our previous magnetically actuated soft capsule endoscopy (MASCE) platform [22]. Fig. 1 shows the prototype of B-MASCE. A fine-needle is attached to the top part of it, and the capsule collapses along its longest dimension in order to deliver the needle out of the bottom part of the capsule. More details of the design will be discussed in Section III.

Fig. 2 shows the overall application scenario. First, B-MASCE is swallowed by a patient. For the protection of the esophagus, the robot is capsuled by ice. After the ice has melted, the capsule can move around inside the stomach to visually inspect the stomach wall with the on-board camera. The stomach is insufflated by carbonated water to ensure free movement of the capsule and a clear view of the surface of the stomach. If a suspicious lesion is found, then B-MASCE is positioned on the lesion's surface, and performs FNC. If multiple lesions are found, each can be biopsied in turn. After the operator has completed the procedure, the capsule is retracted by a thin tether attached to its top body. After the retraction, the needle is taken out and attached to a syringe to remove the tissue inside the needle. The removed tissue is smeared, stained, and fixed on a microscope slide, and sent to the cytology center in a hospital.

III. Design of B-MASCE

A. Design Features

Fig. 3 shows the design features of B-MASCE, which is composed of a fine-needle, a permanent magnet, a four-legged Sarrus linkage, an upper housing, and a lower housing with an anti-slip pattern. The magnet exerts magnetic force and torque to the robot in response to a controlled external magnetic field. The magnetic torque is used to orient the capsule and the magnetic force is used to collapse the Sarrus linkage and deliver the needle through the hole in the bottom of the capsule.

The restoration force from the Sarrus linkage restores the shape of the capsule when the magnetic force is removed. Sinusoidal variation of the axial magnetic force causes repeated smooth motion of the needle in and out of the tissue, which is the required motion for the FNC technique. The Sarrus linkage also restricts the collapsing motion to guide the needle along the axial direction of the capsule, which makes the motion insensitive to slight variations in the applied magnetic fields. The anti-slip pattern on the bottom enhances the friction during the collapsing movement

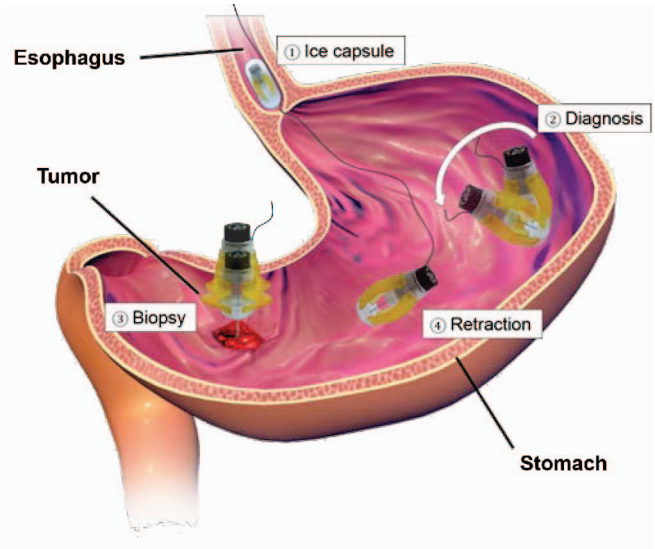


Fig. 2. Application scenario of a thin-tethered B-MASCE. 1) B-MASCE is capsuled by ice, and swallowed. 2) After the ice melts, B-MASCE can move inside the stomach and diagnose. 3) If a lesion is found, B-MASCE moves to the site of the lesion by rolling locomotion, and performs the fine-needle aspiration biopsy. 4) After completing all the tasks, B-MASCE is retracted by a thin tether. (Stomach illustration in background: "Gastric Ulcer" by BruceBlaus / CC BY)

to prevent unintended capsule motion prior to the needle penetration.

B. Design Parameters

Table I shows the design parameters of B-MASCE. In this prototype, the design parameters have been selected to meet the clinical requirements and to prove initial feasibility.

Needle Gauge. Clinical research has shown that 19 gauge (G) to 25 G are recommended [23], [24] to penetrate into tissues and get biopsy samples, and there is no performance difference in the range. For the capsule a 24 G hypodermic needle was chosen that has ⌀0.5652 mm outer diameter and ⌀0.311 mm inner diameter.

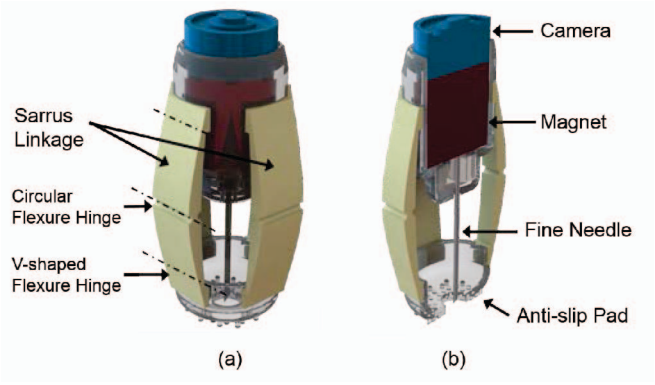


Fig. 3. (a) Exterior of B-MASCE. The Sarrus linkage constraints the axial collapsing motion of the capsule. (b) Section view of B-MASCE. The magnetic force induces the axial movement of the fine-needle along the Sarrus linkage. The anti-slip pad gives additional friction on the surface of the stomach.

TABLE I
DESIGN PARAMETERS

Overall dimension	⌀12 mm × 30 mm
Fine-needle	24 G, 15 mm (length)
Penetration depth	10 mm
Magnet	NdFeB 42 G, ⌀8 × 8 mm^3
Sarrus linkage:	
-Young's modulus	2.07 MPa
-Leg dimension	14 mm (H) × 6 mm (W) × 1.5 mm (D)
-Flexure hinges dimension	Circular: 0.275 mm (D), 0.4 mm (radius)
	V-Shaped: 0.275 mm (D), 135° groove

Penetration Depth. The average stomach thickness is 5.107 mm [25], the average upper GI tumor size is 58 mm (diameter), and the upper GI tumors are visually identifiable at sizes greater than 20 mm diameter [26]. In the case of SMT, the needle penetration depth should be longer than the thickness of the wall, but not so long that the full thickness is pierced. The penetration depth is chosen as 10 mm to meet both criteria.

Magnet Size. The magnet must be large enough to generate sufficient magnetic force and torque. As the size of the capsule is limited, the size of the magnet is chosen to be the maximum size possible inside the capsule's upper body. The magnetic force and torque are controlled by the external magnetic field, which will be discussed in Chapter IV in detail. The magnetic force should be larger than the sum of the restoration force of the Sarrus linkage and the penetration resistance of the targeted tissue. The penetration resistance is different for every tissue and there is no clinical data on stomach tumor tissue. However, as the magnetic force can be adjusted easily by the external magnetic field, this is a matter of tuning for each tissue. In the current state of the research, we have used the penetration resistance of a needle with a liver tissue, which is almost 0.05 N at 10 mm penetration with a 18 G (⌀1.27 mm) needle [27].

Leg Design. The Sarrus linkage leg design is adopted from the previous design shown in [22], [28]–[30]. However, for the biopsy functionality, the linkage must be tuned to ensure that the combined magnetic and linkage forces provide sufficient net force for inserting and retracting the needle. For the design of the linkage, the retraction force is more critical than insertion force, because the insertion force can be safely increased by generating stronger external magnetic field gradients. However, the capsule is designed to retract the needle using only the restoring force of the compliant legs. This is done for safety; if the field gradient were used to retract the needle, it could cause the capsule to suddenly leave the stomach wall, resulting in a momentary loss of control. Thus, we designed the legs to be stiff enough to restore the capsule shape against the tissue's retraction resistance, which is 0.4 N at 10 mm penetration [27].

There are in total twelve hinges in four Sarrus linkage legs. The rotational stiffness of each hinge can be calculated with the equations introduced in [31]. The upper and lower hinges are regarded as V-shaped flexure hinges and the middle one as a circular hinge. Using the values in Table I, the

dimensionless rotational stiffness is expressed as

$$K = \frac{1}{Ebt^2}(\frac{M}{\theta}); K_V = 0.3513; K_C = 0.0643, \quad (1)$$

where K_V and K_C are the dimensionless rotation stiffness values using the empirical fitting data from [31] for V-shaped flexure hinges and circular hinges, respectively, E is the Young's modulus of the material, b is the depth ($z-$direction in Fig. 4a of the hinges), t is the minimum thickness of the hinges, M is the moment on the hinges, and θ is the rotation angle. All the units are in SI unit and *rad*.

The compression force induces torques on the hinges, which results in angle changes in the hinges and a vertical translation of the upper body. Based on the kinematics of the linkages, the relationship between the penetration depth and restoration force of the capsule is expressed as

$$\begin{aligned} F_r &= Ebt^2(8K_V\frac{\theta}{r\sin\theta} + 4K_C\frac{2\theta}{r\sin\theta}); \\ \Delta L &= 2r(1-\cos\theta) \end{aligned} \quad (2)$$

where F_r is the restoration force. Using (2), the restoration force is plotted with the penetration depth in Fig. 4b. The restoration force is always larger than the maximum needle retraction resistive force (0.4 N, 10 mm penetration) [27], the needle will be retracted when the external magnetic force is removed. Although the current design is enough to fulfill the requirements for FNAB, it might be useful to apply magnetic shape programming techniques [32], [33] to the legs for additional functionality.

C. Fabrication

B-MASCE is fabricated with 3D-printing and molding technique. The top and bottom housings are 3D-printed directly (Objet260 Connex3, Stratasys co.). The Sarrus linkage legs are 3D-printed first, and used as a master part for molding. We have used a soft polyurethane elastomer (ST-1060, BJB Enterprise Inc., Young's modulus: 2.07 MPa) as the final material for the legs in the prototype. The detailed recipe is explained in [22]. The fabricated housings and legs are combined using cyanoacrylate glue (LOCTITE 406, Henkel Co.). The hypodermic needle (24 G × 1", B. Braun Co.) is cut to 15 mm length by a nipper, and then inserted into the upper housing. The cut part of the needle remains open. After the needle is inserted, a permanent magnet and a dummy camera are inserted into the upper body.

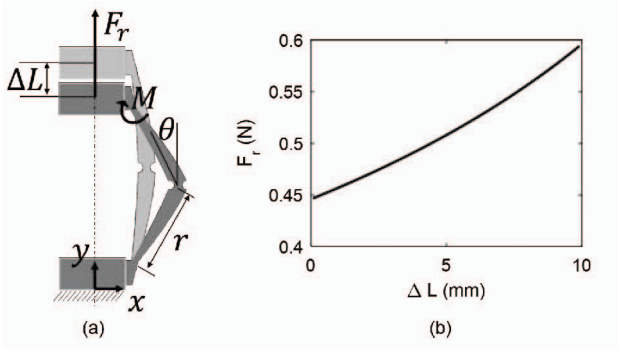


Fig. 4. (a) Diagram for the estimation of restoration force of the capsule by the penetration depth. Counter forces and counter moments are omitted for the visibility. (b) Restoration force along the penetration depth. The legs are designed to overcome the tissue resistance force when the needle is being retracted.

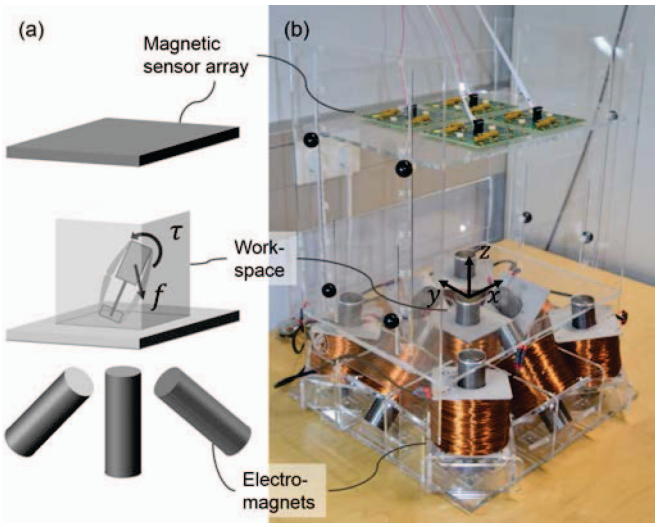


Fig. 5. (a) Schematic diagram of the actuation system. The magnetic sensor array is placed on the top and the electromagnets are placed below. Magnetic fields from the electromagnets generate the magnetic force and torque on the magnet inside B-MASCE. The robot moves inside the workspace. (b) Manufactured actuation setup. Sixty-four three-axis magnetic sensors are placed on the top, and nine electromagnets are placed in the bottom according to the schematic. The coordinate system shows the origin and orientation of the workspace.

IV. Manipulation of B-MASCE

A. Actuation System Description

B-MASCE is manipulated by the external magnetic field, so an accurate means of controlling the B-field and the gradient of the B-field is essential. We have designed an electromagnetic system to control the magnetic field precisely and enhance the safety of the magnetic manipulation. Fig. 5 shows a schematic diagram of the electromagnetic system and a photograph of the assembled setup, which has nine electromagnets and magnetic sensor arrays. The electromagnets are positioned at the bottom and the sensor arrays are positioned at the top. They are separated by enough distance to prevent saturation of the magnetic sensors. The configuration of the electromagnets is optimized to generate a strong z-directional magnetic gradients, and the coils are located in a plane to keep them far enough away from the sensor system. A design framework from OctoMag system [34] is used for the optimization of the magnetic actuation system. However, we added one additional coil to generate a stronger B-field and field gradient, and also to allow the use of redundancy for minimization of the wasted power. In the application of the design framework, we have changed magnetic mapping into non-uniform magnetic fields and its gradient mapping, as the system uses non-uniformity of B-field.

The sensor system is employed to track the position and orientation of B-MASCE. As the actuation is based on non-uniform magnetic fields, the position and orientation information of the capsule are critical to find a proper actuation mapping from the electric current to the magnetic force and torque. The sensor array reads coupled magnetic fields from both B-MASCE and the actuation system. Using an algorithm in [35], the modeled magnetic field from the actuators are removed from the measured magnetic fields, and 5-D position and orientation information of the capsule is calculated using a non-linear optimization algorithm in real-time.

B. Control Methods

The superposition of the magnetic field due to each coil determines the net resultant force and torque on B-MASCE's permanent magnet. The multiple ferrous cores that are close to each other generate coupled magnetic fields. This is because a B-field from one electromagnet becomes additional H-field in the other cores, besides the original H-field from its own coil. These coupling effects should be considered in our setup. A multi-core system's magnetic field and force map from [36] is used here. Using vector and matrix representations, the B-field and force are expressed as

$$\begin{aligned}\mathbf{B}_i &= \frac{\mu_0}{4\pi||\mathbf{p}_i||^3}(3\hat{\mathbf{p}}_i\hat{\mathbf{p}}_i^\top - \mathbb{I})\mathbf{m}_i = \frac{\mu_0}{4\pi}\mathbb{P}_i\mathbf{m}_i \\ \mathbf{F}_i &= \frac{3\mu_0}{4\pi||\mathbf{p}_i||^4}(\mathbf{m}\hat{\mathbf{p}}_i^\top + \hat{\mathbf{p}}_i\mathbf{m}^\top + \\ &\quad (\hat{\mathbf{p}}_i\cdot\mathbf{m})(\mathbb{I} - 5\hat{\mathbf{p}}_i\hat{\mathbf{p}}_i^\top))\mathbf{m}_i = \frac{3\mu_0}{4\pi}\mathbb{F}_i\mathbf{m}_i \quad (3)\end{aligned}$$

where $\mathbf{B}_i$ and $\mathbf{F}_i$ are the B-field and force contribution from the *i*-th electromagnet, μ_0 is the magnetic permeability of free space, $\mathbf{p}_i$ is the displacement vector from the *i*-th electromagnet to the center of the B-MASCE's magnet, $\hat{}$ is the normalization operator to a unit vector, $\mathbb{I}$ is the 3×3 identity matrix, $\mathbf{m}$ is the magnetic moment of the magnet of B-MASCE, $\mathbf{m}_i$ is the magnetic moment of the *i*-th electromagnet; $\mathbb{P}_i$ and $\mathbb{F}_i$ are 3×3 matrices mapping from the magnetic moment of the *i*-th electromagnet to the B-field and force on B-MASCE's magnet, respectively (without permeability and π term).

The superposition of multiple electromagnets' B-fields and forces are expressed in a matrix form as

$$\left[\mathbf{B}^\top, \mathbf{F}^\top\right]^\top = \mathbb{A}\mathbb{D}^{-1}\mathbb{M}\mathbf{I} \quad (4)$$

where, $\mathbf{B}$ is the desired B-field on B-MASCE, $\mathbf{F}$ is the desired magnetic force, and $\mathbf{I}$ is the vector of applied currents in each coil.

$$\mathbb{A} = \frac{\mu_0}{4\pi}\begin{bmatrix}\mathbb{I} & \mathbb{O} \\ \mathbb{O} & 3\mathbb{I}\end{bmatrix}\begin{bmatrix}\mathbb{P}_1 & \cdots & \mathbb{P}_9 \\ \mathbb{F}_1 & \cdots & \mathbb{F}_9\end{bmatrix}$$

is the actuation map which maps from the resultant magnetic moments of the electromagnets to the B-field and magnetic force.

$$\mathbb{D} = \begin{bmatrix}\mathbb{I} & -\frac{V_1}{4\pi}\mathbb{N}_1\mathbb{P}_{12} & -\frac{V_1}{4\pi}\mathbb{N}_1\mathbb{P}_{13} & \cdots \\ -\frac{V_2}{4\pi}\mathbb{N}_2\mathbb{P}_{21} & \mathbb{I} & -\frac{V_2}{4\pi}\mathbb{N}_2\mathbb{P}_{23} & \\ -\frac{V_3}{4\pi}\mathbb{N}_3\mathbb{P}_{31} & -\frac{V_3}{4\pi}\mathbb{N}_3\mathbb{P}_{32} & \mathbb{I} & \\ \vdots & & & \ddots\end{bmatrix}$$

is the magnetic coupling map which encodes the coupling effects among the cores, V_i is the volume of the *i*-th core, $\mathbb{N}_i$ is the *i*-th core's 3×3 external susceptibility matrix (in case of spherical cores: a uniform scale matrix, in the other cases: tensor rotation with directional external susceptibility values in each principal axis) [37] [38], and $\mathbb{P}_{ij}$ is the B-field mapping in (3) by replacing $\mathbf{p}_i$ to a displacement vector from *j*-th core to *i*-th core.

$$\mathbb{M} = \begin{bmatrix}\mathbf{m}_1 & \mathbf{0} & \cdots \\ \mathbf{0} & \mathbf{m}_2 & \\ \vdots & & \ddots\end{bmatrix}$$

is the packing of the magnetic moments of each electromagnets. The required electric current in each coil is achieved using the generalized (Moore-Penrose) pseudo-inverse by minimizing two-norm of the current vector as

$$\mathbf{I} = (\mathbb{A}\mathbb{D}^{-1}\mathbb{M})^\dagger\left[\mathbf{B}^\top, \mathbf{F}^\top\right]^\top. \quad (5)$$

Although the position and orientation information is achieved from the tracking algorithm, the direct usage of the estimated values can cause control instability due to the relatively large orientation error. The orientation of the capsule can change quickly, by pivoting on the substrate, and insufficient bandwidth or accuracy in the estimation of the orientation leads to an incorrect computation since the magnetic moment of the capsule is not known accurately. In such a case, it is simpler to stabilize the system by partitioning the control; the capsule orientation is controlled by assuming that the permanent magnet always aligns with the external field, and the force is controlled independently under the assumption that the orientation tracks perfectly. We applied $||\mathbf{B}|| = 7$ mT with the same direction as the desired orientation of the capsule, and $\mathbf{F} = [0, 0, -0.015]$ N to give enough traction between the robot and the substrate for rolling locomotion.

For the biopsy function, the desired B-field and force are changed due to the required strong force to collapse B-MASCE. We have applied magnetic force ranging from 0.5 N to 0.8 N to give enough collapsing motion over the restoration force (see Fig. 4b). For the jabbing movement, we have varied the applied magnetic force sinusoidally in the range. Those values are determined during the first experiment to tune the fabrication errors (e.g. discrepancy of Young's modulus of legs, thickness of the hinges, uncertain tissue resistance, etc.). Because the very strong magnetic force is exerted on the robot, the desired B-field is also increased to stabilize the robot's orientation effectively. During the experiment, we have found that $||\mathbf{B}|| = 40$ mT is enough to stabilize the robot while FNC is being performed.

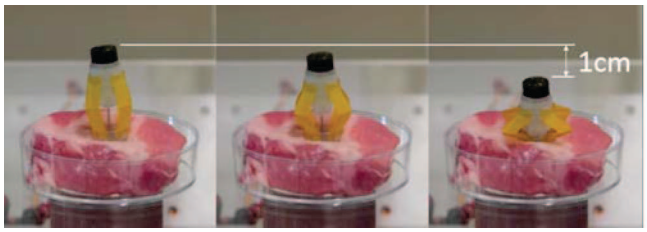


Fig. 6. Collapsing motion of B-MASCE. The magnetic force causes the capsule to collapse, allowing the fine-needle to penetrate inside the tissue.

V. Experiment and Demonstration

We conducted *in vitro* experiments on a fresh pork fat on a plastic anatomical human stomach model (K16, 3B Scientific co.). The pork fat is chosen as a model for a GI tumor as it has a relatively closer structure to a tumor than muscle tissues. The pork fat is cut into two 25 mm diameter slices, and placed onto a Petri dish (first experiment) and into an anatomical human stomach model (demonstration).

The first experiment was conducted to verify the ability of the capsule to perform fine-needle aspiration biopsy. B-MASCE was placed on the tissue sample in the presence of a z-directional B-field, so that it could stand vertically. The gradient of the B-field was slowly increased until a full collapse was observed. The capsule was placed closely to the electromagnet as it requires a strong magnetic force to collapse. Although it is close to the electromagnet, the dipole approximation is still valid with an approximate error of 1% according to [39] (normalized distance: 10 cm / 8 cm = 1.25, axial cylinder magnet case).

Fig. 6 shows one of the experiments on the fat tissue. We have observed that when the magnetic force is higher than the restoration force of the Sarrus linkage legs (Fig. 4b), B-MASCE starts to collapse. As the penetration resistance is significantly smaller than the restoration force, the penetration movement is almost same as collapsing movement of the capsule without the needle. It is found that 0.8N is enough to collapse B-MASCE fully in the current design on the pork fat so that the needle can get deep inside the tissue.

The second experiment was designed to demonstrate the concept of the application scenario. After the capsule is manually placed inside of an anatomical stomach phantom, the demonstration consists of three steps: 1) move to the site of the tumor by rolling locomotion, 2) perform fine-needle capillary biopsy and 3) move back to an area near the starting position. A human operator moved B-MASCE by changing its orientation to induce rolling and performed biopsy changing the force along the axis of the needle. The operator observed the robot's movement and gave commands using a keyboard and a mouse on a visual interface (LabVIEW, National Instruments Co.). The demonstration was done under water to simulate the environment inside the water-insufflated stomach.

Fig. 7 displays the results of the demonstration. During the demonstration, the robot moved relatively slowly (4 seconds for 180° turn) for stable rolling motions. Once the robot had reached the tissue phantom and been vertically oriented, it performed the biopsy by collapsing and recovering its shape. A total of nine jabbing movements were done in 10 seconds and afterwards the capsule was successfully relocated to an area near the starting position. After the demonstration, the robot was retracted by hand and the biopsy sample was examined by a microscope and a camera with a macro lens.

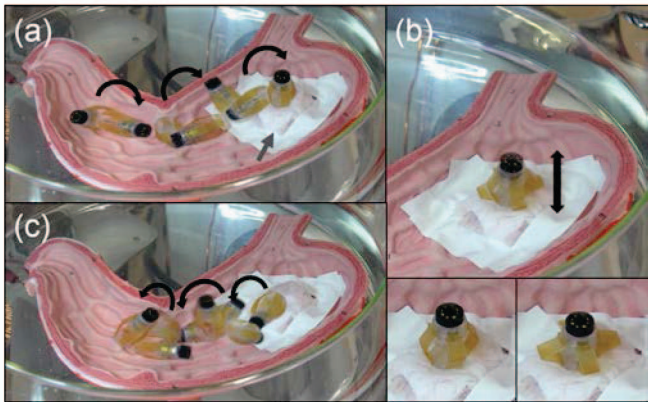


Fig. 7. Demonstration of B-MASCE's rolling locomotion and the biopsy functionality in water (multiple images are overlaid). (a) B-MASCE approaches the site of a fake tumor (gray arrow) by rolling locomotion (black arrow). The pork fat is fixed with white tapes due to the buoyancy. (b) B-MASCE performs fine-needle biopsy with the repetitive collapsing motion (nine times). (c) B-MASCE moves to the other place waiting for the next procedure.

Fig. 8 shows the retracted tissue from the pork fat inside the hollow needle. The tissue was retained inside the needle until the examination as a result of the capillary force. After the retraction of the capsule, a syringe was attached to the fine needle, and the sample was discharged carefully by applying a positive pressure inside the syringe. From the images it is clear that the fat tissue was captured inside the needle. We had repeated the experiment ten times, and could collect the biopsy samples through all the experiments (yield rate: 100%).

VI. Discussion

In this paper, we have proposed and demonstrated the FNC functionality using a magnetically actuated soft capsule endoscope. This is the first trial applying the fine-needle

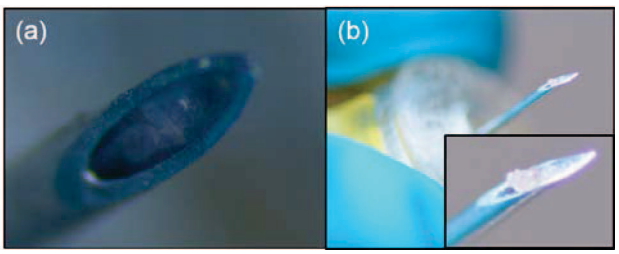


Fig. 8. Biopsy sample inside the fine needle. (a) Optical microscope image before discharging the tissue. The pork fat is seen inside the needle. (b) Obtained sample of the pork fat. The extracted biopsy sample is observed clearly.

biopsy technique to robotic capsule endoscopes, which enables obtaining not only superficial tissues, but also deep tissues undermining the stomach wall, such as submusosal tumors. B-MASCE has the potential to improve the diagnostic accuracy of capsule biopsy procedures in the upper GI tract, and shorten the lesion identification step by performing the diagnosis and biopsy at once.

This new design is simple, but robust to withdraw stomach tissues successfully. By utilizing the single magnet inside the robot for several purposes (locomotion, biopsy, and tracking), the number of system components is minimized, making the capsule design robust and inexpensive to fabricate. By utilizing the soft-polymer Sarrus linkages, the body of the capsule is a hinge, spring element, and encapsulating structure all-in-one. These design elements make B-MASCE significantly less complex than previously proposed biopsy capsule endoscopes, yet still able to operate reliably.

On the other hand, the safety of B-MASCE needs to be considered. The robot is naturally safe due to the Sarrus linkage's restoration force. The only source which can give the collapsing force to the capsule, besides the magnetic force, is the peristalsis from the esophagus and stomach. As the esophagus is narrow, it gives constant pressure to the sides of the capsule when it is being swallowed. As a usual case, the robot is aligned with the esophagus' direction due to its pill-like shape. However, there could be a little chance where the capsule is rotated inside the esophagus and be collapsed by the esophagus' peristalsis. This is the reason for the ice capsule at the first step of the scenario by locking the shape of the capsule. For the retraction of B-MASCE, the tether attached to the capsule plays a role. As the tether is attached to the top part of the capsule, the pulling force aligns the capsule to the direction of the esophagus, which prevents B-MASCE from collapsing during the retraction.

As for the stomach, the environment is different than the esophagus because the stomach is a large cavity and B-MASCE is not compressed by the stomach wall. In clinical applications of capsule endoscopes in the upper GI, it is recommended to drink water with air producing powder [40] to expand the stomach as much as possible. This is for the diagnostic accuracy to see all the lesions, which can be hidden by the wrinkles of the stomach wall. In such a case, the water and the gas inside the stomach prevents the stomach from collapsing and it is safe to use B-MASCE.

However, there are some challenges that remain for future work: control and manipulation issues in the real environment, and registration of the stomach for presentation of the procedure status to the operator. Although the biopsy functionality was demonstrated, the test environment was significantly different than the real one. The real stomach exhibits peristalsis, which disturbs the orientation and position of the robot. In that case, a controller which can robustly reject those disturbances needs to be designed and implemented. Additionally, the stomach wall is extremely slippery due to the mucosa layer. This can cause another control problem, as the pivot point of the rolling locomotion and the supporting point for the bottom pad could move. Especially if the pad slips, the biopsy could be taken in an unintended location. A controller which can align the robot perpendicular to the surface of the stomach precisely and a pad which can give enough static friction need to be further developed.

Additionally, the design of the actuation system is most effective when pulling the capsule's magnet towards the general direction of the iron cores. This particular arrangement is therefore not optimal for biopsy of the superior and inferior surfaces of the stomach. A more complex arrangement of the cores could be designed (e.g., a permanent cores case: [41]) to improve the system for this specific application.

Another necessary addition to the system is a means of registration and localization inside the stomach. For the demonstration, the human operator had to observe the location of the robot visually, which will not be a simple task with only endoscopic video when the capsule is rolling. Ideally, the system should construct an on-line map of the stomach and perform simultaneous localization and mapping to present to the operator an overview of the relative positions of the robot and the stomach, as well as the locations of any identified lesions. The camera on the capsule could be used to gather data for the localization and mapping procedures. There has recently been an effort to adapt techniques for localization of mobile robots to surgical scenarios inside the body [42], which could be incorporated into a capsule endoscopy suite for biopsy.

VII. Conclusion

A magnetically actuated soft capsule endoscope designed for fine-needle aspiration biopsy was described. The integrated fine-needle at the top part of the robot can penetrate into a lesion and capture samples inside the hollow needle using a technique similar to standard clinical procedure. A permanent magnet inside the robot generates a magnetic force and torque through its interaction with an external magnetic field, and it is simultaneously used as a tracking source at the same time. The soft material-based Sarrus linkage works as a needle guide, spring, and body for the capsule. This allows the robot to collapse, deploying the needle into the targeted tissue, and also provides the restoration force for the needle retraction when the external magnetic field is removed. A computer controlled electromagnetic system and magnetic sensor array were employed to control the external magnetic field precisely. Rolling locomotion and biopsy were demonstrated *in vitro* on a plastic stomach model with a swine adipose tissue model. After the demonstration, it was confirmed that a biopsy sample was successfully captured. Precise control techniques, the registration and mapping of the stomach, and *in vivo* demonstration of such a capsule robot with a biopsy tool are areas of system development remaining.

ACKNOWLEDGMENT

The authors want to thank all members at the Physical Intelligence Department, Max Planck Institute for Intelligent

Systems, and especially Dr. Hunter Gilbert for fruitful discussions and suggestions.

REFERENCES

[1] M. Sitti, H. Ceylan, W. Hu, J. Giltinan, M. Turan, S. Yim, and E. Diller, "Biomedical applications of untethered mobile milli/microrobots," in *Proceedings of the IEEE*, vol. 103, no. 2, 2015, pp. 205–224.

[2] A.-M. Singeap, "Capsule endoscopy: The road ahead," *World Journal of Gastroenterology*, vol. 22, no. 1, p. 369, 2016.

[3] G. Ciuti, R. Caliò, D. Camboni, L. Neri, F. Bianchi, A. Arezzo, A. Koulaouzidis, S. Schostek, D. Stoyanov, C. M. Oddo, B. Magnani, A. Menciassi, M. Morino, M. O. Schurr, and P. Dario, "Frontiers of robotic endoscopic capsules: a review," *Journal of Micro-Bio Robotics*, 2016.

[4] J. Driller and G. Neumann, "An Electromagnetic Biopsy Device," *IEEE Transactions on Biomedical Engineering*, vol. 14, no. 1, pp. 52–53, 1967.

[5] K.-C. Kong, J. Cha, D. Jeon, and D.-I. D. Cho, "A rotational micro biopsy device for the capsule endoscope," *2005 IEEE/RSJ International Conference on Intelligent Robots and Systems*, 2005.

[6] K. Kong, S. Yim, S. Choi, and D. Jeon, "A robotic biopsy device for capsule endoscopy," *J. Med. Devices Journal of Medical Devices*, vol. 6, no. 3, p. 031004, 2012.

[7] C. P. Swain, "Method, System and Device for In-vivo Biopsy," Patent US 2008/0 199 065 A1, 2008.

[8] S. Park, K.-i. Koo, S. M. Bang, J. Y. Park, S. Y. Song, and D. D. Cho, "A novel microactuator for microbiopsy in capsular endoscopes," *Journal of Micromechanics and Microengineering*, vol. 18, no. 2, 2008.

[9] W. Chen, G. Yan, S. He, Q. Ke, Z. Wang, H. Liu, and P. Jiang, "Wireless powered capsule endoscopy for colon diagnosis and treatment." *Physiological measurement*, vol. 34, no. 11, pp. 1545–61, 2013.

[10] M. Simi, G. Gerboni, A. Menciassi, and P. Valdastri, "Magnetic torsion spring mechanism for a wireless biopsy capsule," *J. Med. Devices Journal of Medical Devices*, vol. 7, no. 4, p. 041009, 2013.

[11] S. Yim, E. Gultepe, D. Gracias, and M. Sitti, "Biopsy using a magnetic capsule endoscope carrying, releasing and retrieving untethered microgrippers," *IEEE Transactions on Biomedical Engineering*, vol. 61, no. 2, pp. 513–521, 2014.

[12] S. A. Zargar, M. S. Khuroo, R. Mahajan, G. M. Jan, K. Dewani, and V. Koul, "Endoscopic fine needle aspiration cytology in the diagnosis of gastro-oesophageal and colorectal malignancies," *Gut*, vol. 32, no. 7, pp. 745–748, 1991.

[13] D. C. Allen and S. T. Irwin, "Fine needle aspiration cytology of gastric carcinoma." *The Ulster medical journal*, vol. 66, no. 2, pp. 111–114, 1997.

[14] H. Ito, H. Inoue, S. Ryozawa, H. Ikeda, N. Odaka, N. Eleftheriadis, R. Maselli, N. Sando, S. Kimura, and S. E. Kudo, "Fine-needle aspiration biopsy and endoscopic ultrasound for pretreatment pathological diagnosis of gastric gastrointestinal stromal tumors," *Gastroenterology Research and Practice*, vol. 2012, 2012.

[15] H. A. Domanski, *Atlas of fine needle aspiration cytology*. Springer, 2013.

[16] G. Kocjan, *Fine needle aspiration cytology: diagnostic principles and dilemmas*. Springer, 2006.

[17] P. Vilmann and A. Saftoiu, "Endoscopic ultrasound-guided fine needle aspiration biopsy: equipment and technique," *J Gastroenterol Hepatol*, vol. 21, no. 11, pp. 1646–1655, 2006.

[18] M. E. Tublin, J. a. Martin, L. J. Rollin, K. Pealer, M. Kurs-lasky, and N. P. Ohori, "Ultrasound-Guided Fine-Needle Aspiration Versus Fine-Needle Capillary Sampling Biopsy of Thyroid Nodules: Does technique Matter?" *J Ultrasound Med*, vol. 26, no. 12, pp. 1697–1701, 2007.

[19] V. Arantes, R. Logrono, S. Faruqi, I. Ahmed, I. Waxman, and M. S. Bhutani, "Endoscopic sonographically guided fine-needle aspiration yield in submucosal tumors of the gastrointestinal tract," *J Ultrasound Med*, vol. 23, no. 9, pp. 1141–1150, 2004.

[20] T. Kojima, H. Takahashi, A. Parra-Blanco, K. Kohsen, and R. Fujita, "Diagnosis of submucosal tumor of the upper GI tract by endoscopic resection," *Gastrointestinal Endoscopy*, vol. 50, no. 4, pp. 516–522, 1999.

[21] N. Ando, H. Goto, Y. Niwa, Y. Hirooka, N. Ohmiya, T. Nagasaka, and T. Hayakawa, "The diagnosis of GI stromal tumors with EUS-guided fine needle aspiration with immunohistochemical analysis," *Gastrointestinal Endoscopy*, vol. 55, no. 1, pp. 37–43, 2002.

[22] S. Yim and M. Sitti, "Design and rolling locomotion of a magnetically actuated soft capsule endoscope," *IEEE Transactions on Robotics*, vol. 28, no. 1, pp. 183–194, 2012.

[23] K. Hara, N. Mizuno, S. Hijioka, H. Imaoka, M. Tajika, T. Tanaka, M. Ishihara, Y. Niwa, and K. Yamao, "What is the best method for endoscopic ultrasound-guided fine needle aspiration? needle types and aspiration techniques," *Gastrointestinal Intervention*, vol. 3, no. 2, p. 104109, 2014.

[24] K. Webb and J. H. Hwang, "Endoscopic ultrasound-fine needle aspiration versus core biopsy for the diagnosis of subepithelial tumors," *Clinical Endoscopy Clin Endosc*, vol. 46, no. 5, p. 441, 2013.

[25] G. L. Rapaccini, A. Aliotta, M. Pompili, A. Grattagliano, M. Anti, B. Merlino, and G. Gambassi, "Gastric Wall Thickness in Normal and Neoplastic Subjects: A Prospective Study Performed by Abdominal Ultrasound," *Gastrointest Radiol*, vol. 13, no. June 1987, pp. 197–199, 1988.

[26] L. I.-R., C. C.-N., L. M.-T., and L. P.-H., "Surgical treatment of gastric gastrointestinal stromal tumors: analysis of 92 operated patients," *Digestive surgery*, vol. 25, no. 3, pp. 208–212., 2008.

[27] A. M. Okamura, C. Simone, and M. D. O'Leary, "Force modeling for needle insertion into soft tissue," *IEEE Transactions on Biomedical Engineering*, vol. 51, no. 10, pp. 1707–1716, 2004.

[28] S. Yim and M. Sitti, "Shape-programmable soft capsule robots for semi-implantable drug delivery," *IEEE Transactions on Robotics*, vol. 28, no. 5, pp. 1198–1202, Oct. 2012.

[29] S. Yim, K. Goyal, and M. Sitti, "Magnetically actuated soft capsule with the multimodal drug release function," *IEEE transactions on Mechatronics*, vol. 18, no. 4, pp. 1413–1418, 2013.

[30] S. Yim and M. Sitti, "3-D localization method for a magnetically actuated soft capsule endoscope and its applications," *IEEE Transactions on Robotics*, vol. 29, no. 5, pp. 1139–1151, 2013.

[31] Y. Tian, B. Shirinzadeh, D. Zhang, and Y. Zhong, "Three flexure hinges for compliant mechanism designs based on dimensionless graph analysis," *Precision Engineering*, vol. 34, no. 1, pp. 92–100, 2010.

[32] E. Diller, J. Zhuang, G. Zhan Lum, M. R. Edwards, and M. Sitti, "Continuously distributed magnetization profile for millimeter-scale elastomeric undulatory swimming," *Applied Physics Letters*, vol. 104, no. 17, 2014.

[33] G. Z. Lum, Z. Ye, X. Dong, H. Marvi, O. Erin, W. Hu, and M. Sitti, "Shape-programmable magnetic soft matter." *Proceedings of the National Academy of Sciences of the United States of America*, vol. 113, no. 41, pp. E6007–E6015, 2016. [Online]. Available: http://www.ncbi.nlm.nih.gov/pubmed/27671658

[34] M. P. Kummer, J. J. Abbott, B. E. Kratochvil, R. Borer, A. Sengul, and B. J. Nelson, "OctoMag: An Electromagnetic System for 5-DOF Wireless Micromanipulation," *IEEE Transactions on Robotics*, vol. 26, no. 6, pp. 1006–1017, dec 2010.

[35] D. Son, S. Yim, and M. Sitti, "A 5-D Localization Method for a Magnetically Manipulated Untethered Robot Using a 2-D Array of Hall-Effect Sensors," *IEEE/ASME Transactions on Mechatronics*, vol. 21, no. 2, pp. 708–716, 2016.

[36] A. J. Petruska, J. B. Brink, and J. J. Abbott, "First Demonstration of a Modular and Reconfigurable Magnetic-Manipulation System," in *Robotics and Automation (ICRA), 2015 IEEE International Conference on*, Seattle, WA, 2015, pp. 149 – 155.

[37] J. Osborn, "Demagnetizing Facotrs of the General Ellipsoid," *Physical Review*, vol. 67, no. h 8, p. 351, 1945.

[38] D. X. Chen, E. Pardo, and A. Sanchez, "Fluxmetric and magnetometric demagnetizing factors for cylinders," *Journal of Magnetism and Magnetic Materials*, vol. 306, no. 1, pp. 135–146, 2006.

[39] A. J. Petruska and J. J. Abbott, "Optimal permanent-magnet geometries for dipole field approximation," *IEEE Transactions on Magnetics*, vol. 49, no. 2, pp. 811–819, feb 2013.

[40] H.-L. Ching, M. F. Hale, and M. E. McAlindon, "Current and future role of magnetically assisted gastric capsule endoscopy in the upper gastrointestinal tract," *Therapeutic Advances in Gastroenterology*, vol. 9, no. 3, pp. 313–321, 2016.

[41] F. Munoz, G. Alici, W. Li, and M. Sitti, "Size Optimization of a Magnetic System for Drug Delivery with Capsule Robots," *IEEE Transactions on Magnetics*, vol. 52, no. 5, 2016.

[42] S. T. Tully, "BodySLAM: localization and mapping for surgical guidance," Ph.D. dissertation, Carnegie Mellon University, 2012.